frontiers in Materials

ORIGINAL RESEARCH
published: 16 September 2016
doi: 10.3389/fmats.2016.00043

Microstructural Changes Induced by CO_2 Exposure in Alkali-Activated Slag/Metakaolin Pastes

*Susan A. Bernal**

Department of Civil and Structural Engineering, The University of Sheffield, Sheffield, UK

The structural changes induced by accelerated carbonation in alkali-activated slag/metakaolin (MK) cements were determined. The specimens were carbonated for 540 h in an environmental chamber with a CO_2 concentration of 1.0 ± 0.2%, a temperature of 20 ± 2°C, and relative humidity of 65 ± 5%. Accelerated carbonation led to decalcification of the main binding phase of these cements, which is an aluminum substituted calcium silicate hydrate (C-(N-)A-S-H) type gel, and the consequent formation of calcium carbonate. The sodium-rich carbonates trona ($Na_2CO_3{\cdot}NaHCO_3{\cdot}2H_2O$) and gaylussite ($Na_2Ca(CO_3)_2{\cdot}5H_2O$) were identified in cements containing up to 10 wt.% MK as carbonation products. The formation of these carbonates is mainly associated with the chemical reaction between the CO_2 and the free alkalis present in the pore solution. The structure of the carbonated cements is dominated by an aluminosilicate hydrate (N-A-S-H) type gel, independent of the MK content. The N-A-S-H type gels identified are likely to be derived both from the activation reaction of the MK, forming a low-calcium gel product that does not seem to undergo structural changes upon CO_2 exposure, and the decalcification of C-(N-)A-S-H type gel. The carbonated pastes present a highly porous microstructure, more notable as the content of MK content in the cement increases, which might have a negative impact on the durability of these materials in service.

Keywords: alkali-activation, blast furnace slag, metakaolin, accelerated carbonation

OPEN ACCESS

Edited by:
Wenhui Duan,
Monash University, Australia

Reviewed by:
Denvid Lau,
City University of Hong Kong, Hong Kong
Jiafei Jiang,
Tongji University, China

***Correspondence:**
Susan A. Bernal
s.bernal@sheffield.ac.uk

Specialty section:
This article was submitted to Structural Materials, a section of the journal Frontiers in Materials

Received: *11 July 2016*
Accepted: *02 September 2016*
Published: *16 September 2016*

Citation:
Bernal SA (2016) Microstructural Changes Induced by CO_2 Exposure in Alkali-Activated Slag/Metakaolin Pastes. Front. Mater. 3:43. doi: 10.3389/fmats.2016.00043

INTRODUCTION

Alkali-activated cements are a class of cements produced at room temperature via a chemical reaction between a poorly crystalline aluminosilicate material (termed the *precursor*) and a highly alkaline solution (the *activator*) to form hardened solids, if properly formulated and cured (Provis and Bernal, 2014). Alkali-activated cements based on Ca-rich precursors, such as granulated blast furnace slag (GBFS), a by-product of the iron manufacturing industry, are currently used for production of mortars and concretes for structural and non-structural applications (Juenger et al., 2011; Buchwald et al., 2015). Alkali-activated cements are considered to be an environmentally sustainable construction material, and so research in this area has for several years been driven by the Greenhouse and economic benefits that can be gained from a more sustainable construction materials industry (Habert et al., 2011). There is a general consensus that alkali-activated cements can offer cradle-to-gate Greenhouse emissions savings approaching 40–80% compared to Portland cement for a performance-equivalent material. However, the question of whether mortars and concretes produced with these alternative binders can

withstand the test of time during their service life requires further analysis. These materials do not yet have the long-term performance record of conventional Portland cement, and there is not yet a full understanding of the factors governing their durability.

Carbonation is understood as an acid–base reaction between the hydrated products formed in a cement, and the carbonic acid formed by dissolution of atmospheric CO_2 in the pore solution, leading to the formation of carbonates (Hobbs, 2001; Sanjuán et al., 2003; Fernández-Bertos et al., 2004). In addition to causing matrix degradation, carbonation is also one of the key processes that can cause corrosion of steel rebar within concretes in service environments that do not involve chloride attack. Therefore, if alkali-activated slag cements and concretes are going to play an important role in future infrastructure development, they need to perform as well as, or better than, Portland cements under service conditions.

The susceptibility to carbonation of alkali-activated slag cements has been identified as one of their potential disadvantages, compared with Portland cement, as earlier studies assessing the degradation of these materials under exposure to high CO_2 concentrations showed notable structural changes that might compromise mechanical performance (Deja, 2002; Palacios and Puertas, 2006; Puertas et al., 2006). The accelerated carbonation of alkali-activated binders is mainly a chemically controlled mechanism (Bernal, 2014), and its extent is governed by similar parameters to those which promote specific microstructural characteristics in these materials, such as the type of the precursor used (aluminosilicate or GBFS) (Bernal et al., 2013a, 2014a), and the nature of the activator (Palacios and Puertas, 2006). The testing conditions, such as relative humidity and CO_2 concentration, also have a significant impact on the rate and extent of carbonation of alkali-activated materials. This is mainly associated with the nature of the products derived from the pore solution carbonation, and also the desiccation and consequent cracking these materials undergo during the usual conditioning (involving exposure to a drying atmosphere) prior to accelerated carbonation testing (Bernal, 2014; Yang et al., 2016). Despite the apparent high susceptibility to carbonation, which has been reported for alkali-activated cements under laboratory conditions, no correlation has been identified between results obtained when exposing these materials to a high CO_2 concentration via accelerated testing methods, and under exposure to atmospheric carbonation conditions for several years (Bernal et al., 2014b). This elucidates that the use of accelerated testing methods to assess carbonation of alkali-activated slags can underestimate the real performance these materials will have during service life.

The addition of a small amount of metakaolin (MK) (up to 20 wt.%) to slag-rich silicate-activated binders promotes the formation of a structure mainly composed of coexisting alkali aluminosilicate and Al-substituted calcium silicate hydrate (C-A-S-H) type gels (Bernal et al., 2012a). The addition of up to 20 wt.% MK to alkali-activated slag cements does not have a notable impact in their mechanical performance, but in the case of highly reactive slags, it contributes to the ability to control the setting time (Bernal et al., 2010). When using high doses of activator (>5% Na_2O by mass of GBFS + MK), a C-A-S-H type gel is formed as the main binding phase (Bernal et al., 2013b). Concretes and mortars produced with these high activator dose slag/MK blends developed high compressive strengths when compared to reference alkali-activated slag systems (Bernal et al., 2012a; Bernal, 2015). The inclusion of MK induced negligible changes in the compressive strength of mortars post-carbonation, although reductions in porosity were observed (Bernal, 2015). Conversely, in concretes, exposure to high CO_2 concentrations led to a reduction of loading capacity, and increased porosity (Bernal et al., 2014b). These divergent results are most likely a consequence of the changes in permeable voids between mortars and concretes, leading to different rates of carbonation and extents of microstructural changes for a given time of CO_2 exposure.

To further elucidate the role of the microstructural features of these carbonated binders in determining the performance of mortars and concretes produced with alkali-activated slag/MK binders, this study focusses on assessing the structural changes induced by high CO_2 exposure of alkali-activated slag/MK pastes, under controlled environmental conditions, using high-resolution X-ray diffraction (XRD), thermogravimetry, Fourier transform infrared (FTIR) spectroscopy, and scanning electron microscopy (SEM).

EXPERIMENTAL PROGRAM

Materials

The primary raw material used was a blast furnace slag with a specific gravity of 2900 kg/m^3 and Blaine fineness 399 m^2/kg. The particle size range, determined through laser diffraction, was 0.1–74 μm, with an average particle size, d_{50}, of 15 μm. The chemical composition of this slag is shown in **Table 1**.

The MK used was produced in the laboratory by calcination of a kaolin containing minor quartz and dickite impurities, at 700°C in air, for 2 h. The particle size range of the MK was 1.8–100 μm, with a d_{50} of 13.2 μm and 10% of particles finer than 4 μm. Alkaline activating solutions were formulated by blending a commercial sodium silicate solution with 32.4 wt.% SiO_2, 13.5 wt.% Na_2O, and 54.1 wt.% H_2O, together with 50 wt.% NaOH solution, to reach the specified activator compositions.

Sample Synthesis and Test Procedure

Pastes with different GBFS/(GBFS + MK) ratios and with a constant water/solids ratio of 0.23 (where "solids" is defined as GBFS + MK + anhydrous activator) were produced using the

TABLE 1 | Composition of the GBFS and MK used, determined through X-ray fluorescence analysis.

Precursor	Component (mass% as oxide)						
	SiO_2	Al_2O_3	CaO	Fe_2O_3	MgO	Other	LOI
GBFS	32.3	16.3	42.5	2.4	2.9	1.7	1.9
MK	50.7	44.6	2.7	–	–	1.0	1.0

LOI is loss on ignition at 1000°C.

TABLE 2 | Mix designs of the pastes studied.

Component	Overall SiO_2/Al_2O_3 molar ratio		
	4.4	4.0	3.6
GBFS	1	0.9	0.8
MK	–	0.1	0.2
Sodium silicate solution	0.3	0.3	0.3
NaOH (50 wt.% solution)	0.2	0.2	0.2
Water	0.3	0.3	0.3
Activator concentration (% Na_2O by mass of GBFS + MK)	10.6	11.6	12

activation conditions described in **Table 2**. The specimens were cast in a cylindrical mold and stored in hermetically sealed containers with a relative humidity of 90% and a temperature of 25 ± 2°C for 28 days.

Pastes were then crushed and sieved to a particle size of 0.074 mm, and exposed to CO_2 using an accelerated carbonation chamber with a CO_2 concentration of 1.0 ± 0.2%, a temperature of 20 ± 2°C, and RH = 65 ± 5%. These accelerated carbonation conditions were selected based on a previous study (Bernal et al., 2012b), where it was demonstrated that comparable carbonation reaction products to those forming after several years of atmospheric exposure are identified in samples carbonated under these conditions. Non-carbonated samples, and samples exposed to CO_2 for 540 h (referred to as carbonated throughout the document) were analyzed through:

- X-ray diffraction was carried out using a high-resolution high-throughput synchrotron powder X-ray diffractometer with a system of 12 simultaneous analyzer/detectors, at beamline 11-BM at the Advanced Photon Source (APS), Argonne National Laboratory (USA). The tests were conducted according to the standard protocols for automated data acquisition on the 11-BM beamline. The conditions for the data collection were: continuous scanning of a detector covering an angular range of 20° with a step rate of 0.01°/s, a step size of 0.001° and wavelengths of $\lambda = 0.401738$ Å for non-carbonated samples, and 0.458879 Å for carbonated samples. Data have been converted to Q units ($Q = 4\pi \sin\theta/\lambda$) for presentation here, to enable comparison between data sets collected at different wavelengths.
- Fourier transform infrared spectrometry was conducted via the KBr pellet technique, using a Shimadzu FTIR 8400 instrument, scanning from 4000 to 400 cm^{-1}.
- Thermogravimetry was carried out in a SDT-Q600 TGA/DSC from TA Instruments. Samples were tested from 25 to 1100°C, in a nitrogen atmosphere, at a heating rate of 10°C/min.
- Scanning electron microscopy of non-carbonated samples was carried out in a Philips XL30F Field Emission SEM, with an accelerating voltage of 15 kV, and a working distance of 10 mm.
- Environmental scanning electron microscopy (ESEM) of unpolished carbonated samples was conducted using an FEI Quanta instrument with a 15 kV accelerating voltage and a working distance of 10 mm, in low vacuum mode.

RESULTS AND DISCUSSION

High-Resolution Synchrotron X-Ray Diffraction

High-resolution X-ray diffractograms of non-carbonated pastes of the compositions studied here, as a function of the curing time, were previously reported by Bernal et al. (2013b). As the main partially crystalline reaction products, tobermorite-type phases with three different basal spacings (9, 11, and 14 Å) were observed in these cements, most likely with some Al substitution (Myers et al., 2013). A sodium calcium silicate hydrate ($Na_2Ca_2Si_2O_7{\cdot}H_2O$; Powder Diffraction File (PDF) # 00-022-0891), and two aluminosilicate zeolite products, gismondine ($CaAl_2Si_2O_8{\cdot}4H_2O$; PDF # 00-020-0452), and garronite ($NaCa_{2.5}(Si_{10}Al_6)O_{32}{\cdot}13H_2O$; PDF # 99-000-1300), the last of which was solely identified in specimens containing MK. Variations in the intensities of the reflections of some of these phases were observed as a function of the MK content, which is discussed in detail by Bernal et al. (2013b). Other crystalline phases, including gehlenite ($Ca_2Al_2SiO_7$, PDF # 00-035-0755), quartz (SiO_2) (PDF #01-078-2315), and calcite ($CaCO_3$) (PDF# 01-072-1214), attributed to the unreacted slag, were also observed.

Upon CO_2 exposure, samples with GBFS/(GBFS + MK) = 1.0 (**Figure 1A**) showed the formation of the sodium carbonate trona ($Na_2CO_3{\cdot}NaHCO_3{\cdot}2H_2O$) (PDF #00-029-1447), associated with the carbonation of the pore solution present in the sample (Bernal et al., 2012b), along with minor traces of the sodium-calcium carbonate gaylussite ($Na_2Ca(CO_3)_2{\cdot}5H_2O$, PDF# 00-012-0255). This double salt has been identified as a carbonation product in some alkali-activated slag cements (Bernal et al., 2012b, 2013a), although was not observed in a study of carbonated samples produced with a similar slag to that used in this study, but activated with a lower activator dose (Bernal et al., 2010). A notable increase in the intensity of the reflections assigned to calcite was observed, along with reduction in the intensities of the reflections assigned to the Al-substituted C-S-H and C-(N-)S-H type phases. This demonstrates that the exposure of these cements to high concentrations of CO_2 is leading to decalcification of the main binding reaction products, toward formation of calcium carbonates, as has been reported for Ca-rich alkali-activated cements (Palacios and Puertas, 2006). Changes in the reflection assigned to the zeolites gismondine and garronite were not observed upon CO_2 exposure. The fact that traces of C-S-H type phases are still identifiable in the diffraction data for the carbonated samples indicates that the pastes are not yet fully carbonated after 540 h of CO_2 exposure.

Similar results to those observed in samples solely based on slag (**Figure 1A**) were identified in carbonated samples with GBFS/(GBFS + MK) = 0.9 (**Figure 1B**). This suggests that the substitution of slag by MK in a low quantity (≥10 wt.%) does not induce notable changes in the phase assemblages of these alkali-activated cements. Conversely, in samples with GBFS/(GBFS + MK) = 0.8, neither trona nor gaylussite were identified as carbonation products, although these pastes were produced with the highest activator Na_2O concentration among the cements studied (**Table 2**). This might be associated with the higher degree

of consumption of alkalis via the activation reaction of MK, reducing the amount of free alkalis in the pore solution of these cements, and consequently supressing the formation of Na-rich carbonates.

Thermogravimetry

In non-carbonated pastes (**Figure 2A**), the main weight loss is identified below 250°C, and is more notable in pastes with higher MK contents. The weight loss in this temperature range is

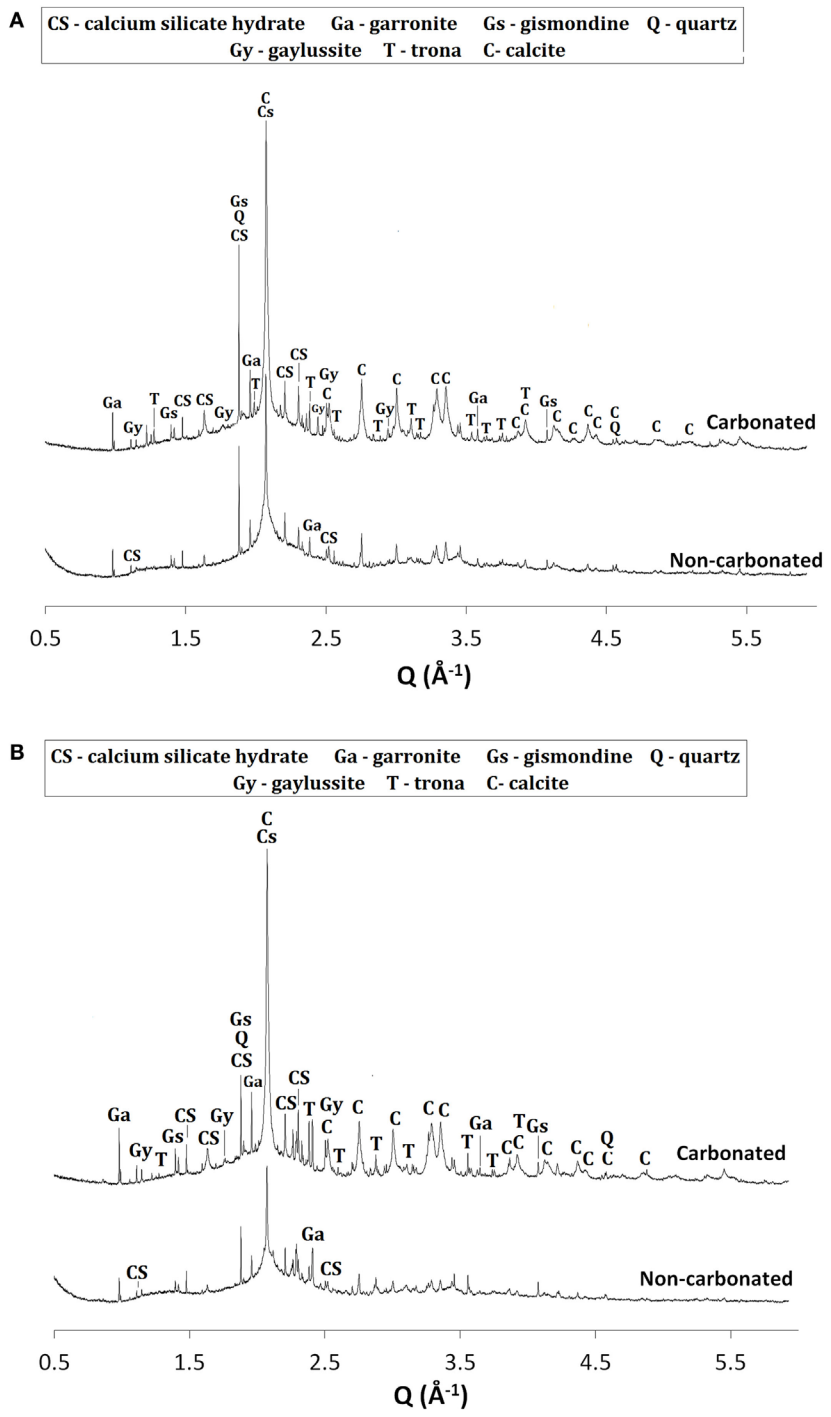

FIGURE 1 | High-resolution synchrotron X-ray diffraction patterns of non-carbonated from Bernal et al. (2013b) and accelerated-carbonated alkali-activated pasted with a GBFS/(GBFS + MK) of (A) 1.0, (B) 0.9, and (C) 0.8.

(Continued)

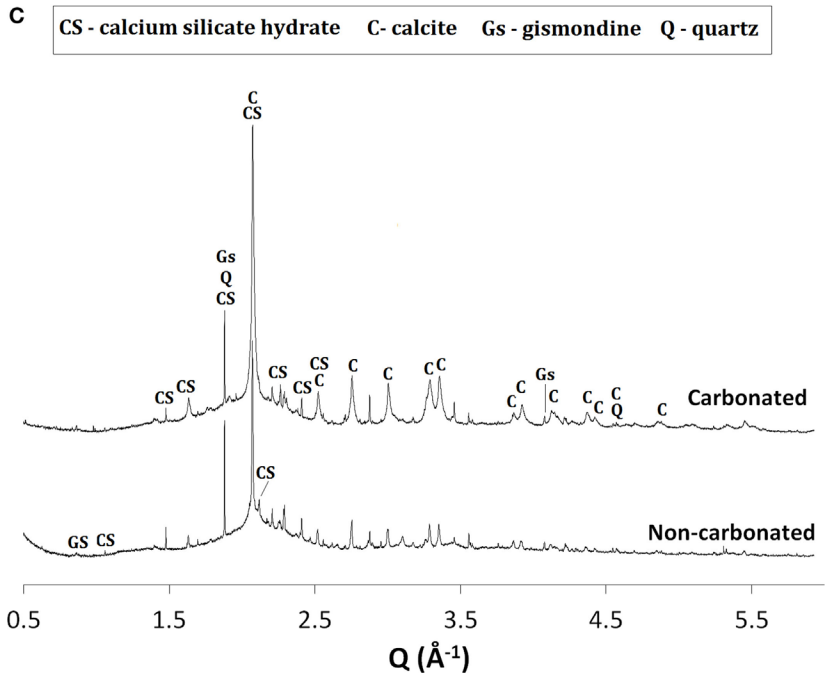

FIGURE 1 | **Continued.**
Peaks marked as CS are assigned to tobermorite-type phases with the three different basal spacings as well as the Na-containing C-S-H.

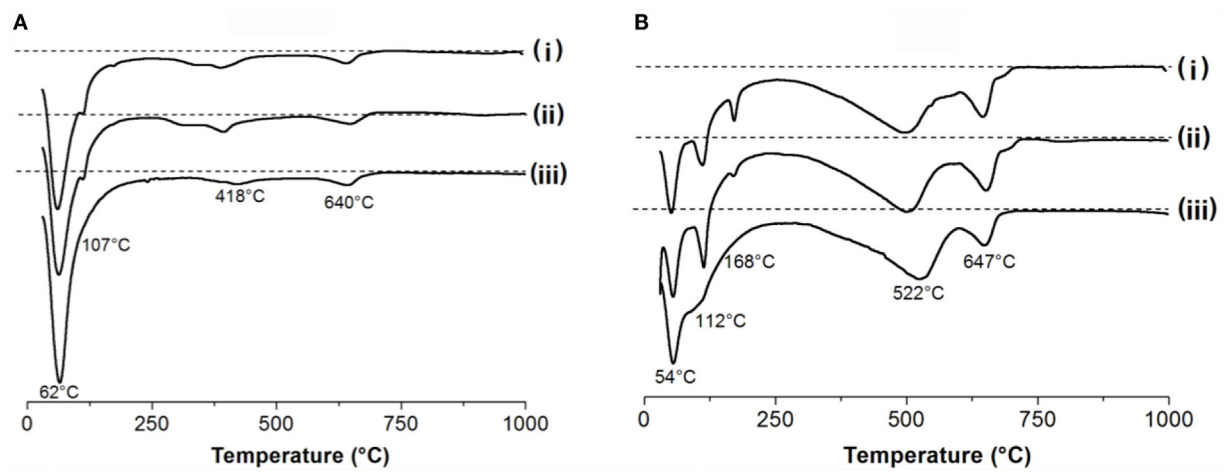

FIGURE 2 | **Thermogravimetry curves and differential thermograms of (A) non-carbonated and (B) accelerated-carbonated alkali-activated pasted with a GBFS/(GBFS + MK) of (i) 1.0, (ii) 0.9, and (iii) 0.8**.

attributed to the evaporation of loosely bound water in the system, and dehydration of the substituted tobermorite-type (C-(N-) A-S-H) gel (Alarcon-Ruíz et al., 2005) present in these pastes. The temperature at which the weight loss is most rapid (i.e., the minimum in the differential thermograms plotted in **Figure 2**) is similar for the three samples at 62°C, in good agreement with results previously identified for alkali-activated GBFS/MK systems with high slag content, where the structure of the binders is dominated by the activation of the slag (Buchwald et al., 2007; Bernal et al., 2011a). The fact that more weight is lost by samples with GBFS/(GBFS + MK) = 0.8 might indicate that water is more loosely bound in the reaction products forming in this paste. The small peak observed at 107°C in the data for samples with GBFS/(GBFS + MK) = 1.0 and 0.9 is attributed to the dehydration of the zeolite gismondine (Bernal et al., 2011a), identified as one of the main crystalline reaction products in activated GBFS/MK under the activation conditions used in this study (Bernal et al., 2013b). Gismondine was not observed as a reaction product in

pastes with 20 wt.% MK (Bernal et al., 2013b), consistent with the thermogravimetry results presented here.

The peaks between 400°C and 418°C cannot be assigned to any crystalline phase present in these systems. The recent results of L'Hôpital et al. (2016) suggest that a weight loss in this temperature range most likely corresponds to dehydration of alkali-containing C-A-S-H type gels, such as those forming in the pastes assessed here. The peak at 640°C is assigned to calcium carbonate present in the anhydrous GBFS as a result of weathering prior to sample synthesis (Bernal et al., 2010). Negligible weight changes were observed above 700°C.

In carbonated samples (**Figure 2B**), an initial weight loss band centered at 52°C is identified in all of the samples. Carbonation of alkali-activated slags leads to decalcification of the C-(N-)A-S-H type gels forming in these systems, resulting in the formation of an aluminosilicate hydrate type gel (Bernal et al., 2013a, 2014a), whose water is more loosely bound than in the original C-(N-)A-S-H. This might be inducing the shift toward lower temperatures of this weight loss peak compared to the uncarbonated samples. In specimens with GBFS/(GBFS + MK) ratios of 1.0 and 0.9 a peak at 112°C was observed, and assigned to trona, which is one of the main carbonate product forming in these binders as identified by XRD (**Figure 1**). Barall and Rogers (1966) identified that the thermal decomposition of trona takes place in two stages, as shown in Eqs 1 and 2. The first decomposition stage leads to weight losses at ~110°C, while decomposition of the sodium bicarbonate leads to weight losses at slightly higher temperatures (~123°C).

$$Na_2CO_3 \cdot NaHCO_3 \cdot 2H_2O \rightarrow Na_2CO_3 + NaHCO_3 + 2H_2O \quad (1)$$

$$2NaHCO_3 \rightarrow Na_2CO_3 + CO_2 + H_2O \quad (2)$$

A peak centered at 168°C is also identified in pastes with a GBFS/(GBFS + MK) of 1.0 and 0.9, whose intensity reduced with the inclusion of MK in the binders. A less resolved peak has been identified at a similar temperatures in accelerated-carbonated alkali-activated slag cements (Bernal et al., 2013a), and assigned to decomposition of hydrous sodium–calcium carbonates [e.g., gaylussite or pirssonite (Johnson and Robb, 1973)]. In the samples assessed, traces of gaylussite were identified by high-resolution XRD (**Figure 1**) and, therefore, this weight loss is assigned to decomposition of this phase. In samples with GBFS/(GBFS + MK) = 0.8, peaks associated with decomposition of the sodium carbonate products were not observed, in accordance with the high-resolution XRD results (**Figure 1**).

Fourier Transform Infrared Spectroscopy

In non-carbonated samples solely based on slag (**Figure 3A**), a band at 1645cm^{-1} is observed, assigned to the bending vibration mode of the H-OH bonds in the reaction products forming. The band centered at 1414 cm^{-1} is attributed to the asymmetric stretching mode of the O-C-O bonds of CO_3^{2-} ions of the calcite present in the unreacted slag. The asymmetric stretching resonance of the Si-O-T bonds (where T can be Si or Al) was observed at 968 cm^{-1},

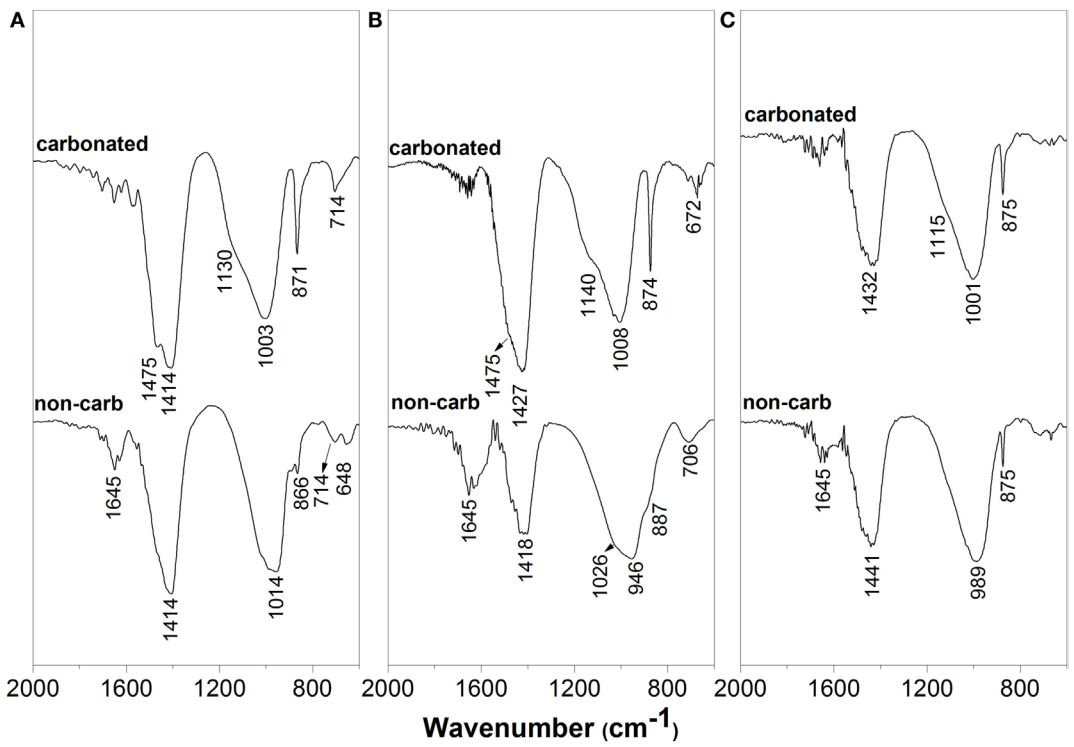

FIGURE 3 | FTIR spectra of non-carbonated and accelerated-carbonated alkali-silicate-activated slag/metakaolin pastes with GBFS/(GBFS + MK) ratios of (A) 1.0, (B) 0.9, and (C) 0.8.

along with a shoulder at 866 cm^{-1} assigned to the vibration mode of the Al-O bonds of the AlO_4^- groups in the reaction products. The Si-O-T band position is characteristic of the environments of silicon tetrahedra (SiO_4) in the chain structure of C-S-H type gels (García Lodeiro et al., 2009). The band centered at 714 cm^{-1} corresponds to the bending vibration mode of the Al-O-Si bonds, and the band at 648 cm^{-1} is attributed to the symmetric vibration mode of the Si-O-Si or Al-O-Si bonds. This band corresponds to C-A-S-H type phases, and the zeolites gismondine and garronite forming in these systems, as identified by XRD (**Figure 1**). This band has also been observed in unreacted slag (Bernal et al., 2011b), and has been attributed to gehlenite. All infrared band assignments follow references (Huang and Kerr, 1960; Farmer, 1974; Gadsden, 1975; Sitarz et al., 2000a,b).

The addition of 10 wt.% MK [i.e., GBFS/(GBFS + MK) = 0.9] led to a reduction in intensity of the O-C-O band centered at 1418 cm^{-1}, consistent with the lower content of slag in these cements. In the region of the Si-O-T vibration modes, two overlapping bands at 1026 and 957 cm^{-1} were identified. A higher wavenumber for the asymmetric stretching Si-O-T bonds is related to increased polymerization degree of the C-S-H type gels (Yu et al., 1999), but this effect is counteracted when the Al supplied by MK is incorporated into this gel, which shifts the Si-O-T band toward lower wavenumbers (Bernal et al., 2011b). Myers et al. (2015) identified highly polymerized silicate sites $Q^4(3Al)$ and $Q^4(4Al)$ in alkali-activated slags via high-resolution NMR spectroscopy, indicating the formation of a disordered aluminosilicate product resembling an alkali aluminosilicate (hydrate) (N–A–S(–H)) type gel, typically observed in MK geopolymers (Williams et al., 2011), along with the C-(N-)A-S-H type gels. Therefore, the two peaks identified in the Si-O-T region of the slag/MK cement spectrum (**Figure 3B**) cannot be assigned to a specific phase, but most likely correspond to the highly crosslinked C-(N-)A-S-H type gels typically identified in alkali-activated slag cements (Myers et al., 2015), and potentially to a secondary N-A-S-H type gel derived from the activation of both slag and MK, and structurally related to the zeolites present in the samples. The shoulder at 887 cm^{-1} along with a peak at 706 cm^{-1} are assigned to the Al-O and Al-O-Si bonds that can be present in C-(N-)A-S-H and/or N-A-S-H type gels.

The addition of 20 wt.% MK [i.e., GBFS/(GBFS/MK) = 0.8], **Figure 3C**, also led to the shifting of the T-O-T band, which is more symmetric than in samples with lower MK content and observed at 989 cm^{-1}, along with the formation of a well-resolved peak at 875 cm^{-1} assigned to calcite. The fact that a sole band is identified in this spectrum might suggest that there are less differences either in chemistry and/or structure (e.g., degree of crosslinking) of the C-(N-)A-S-H and N-A-S-H type gels forming in these cements as the MK content increases.

Upon accelerated carbonation (**Figure 3A**), in cements solely based on slag, a shoulder centered at 1475 cm^{-1} is identified along with the asymmetric stretching vibration band of the CO_3^{2-} groups at 1414 cm^{-1}. This secondary carbonate band is assigned to trona (Huang and Kerr, 1960), which was identified by XRD (**Figure 1**). Between 1100 and 900 cm^{-1}, formation of a secondary band centered at 1130 cm^{-1} is observed, along with a slight sift of the T-O-T band from 1014 to 1003 cm^{-1}. Accelerated carbonation of alkali-activated slags cements leads to decalcification of the C-A-S-H type gels (Palacios and Puertas, 2006), and higher wavenumbers can be associated with a high degree of polymerization of silicates. This is consistent with the formation of aluminosilicate hydrate type gels, which present bands at similar wavenumbers (García-Lodeiro et al., 2008) to those identified in the carbonated pastes. The sharp peak identified at 871 cm^{-1} is assigned to calcite, also identified by XRD (**Figure 1**). A slight increase in the intensity of the band at 714 cm^{-1}, associated with the bending vibration mode of the Al-O-Si bonds, was also observed. This suggests an increase in the fraction of Al-O-Si bonds within this paste, consistent with the formation of N-A-S-H type gel in this cement upon CO_2 exposure (Bernal et al., 2013a).

In carbonated pastes containing 10 wt.% MK (**Figure 3B**), similar bands to those identified in the formulation solely based on slag were observed. In this case, the T-O-T band shifted from 946 cm^{-1} in non-carbonated samples to 1008 cm^{-1} in carbonated specimens, along with the formation of a distinct shoulder at 1140 cm^{-1}. Upon accelerated carbonation of Ca-free alkali-activated cements, changes in the structure of the N-A-S-H type gel have not been identified (Bernal et al., 2013a); therefore, the changes in the position of the T-O-T band are assigned to the decalcification of the C-(N-)A-S-H type gel. The two distinct peaks correspond to N-A-S-H type gels (García-Lodeiro et al., 2008) and the vibration mode identified at 642 cm^{-1} is assigned to vibrations of rings present in this type of gel (Mozgawa et al., 2002).

In carbonated pastes with a GBFS/(GBFS + MK) ratio of 0.8 (**Figure 3C**), the band at 1475 cm^{-1} assigned to trona was not identified, consistent with the XRD (**Figure 1C**) and TGA (**Figure 2B**) results. Similar to the pastes with 10 wt.% MK (**Figure 3B**), two bands at 1001 and 1115 cm^{-1} are observed in the carbonated samples, consistent with the formation of N-A-S-H type gels. A slight increase in the intensity of the peak at 875 cm^{-1} assigned to calcite is observed in the carbonated sample.

Scanning Electron Microscopy

Non-carbonated samples based solely on slag present a highly dense, smooth, and continuous microstructure (**Figure 4A**), consistent with the results typically reported for these materials (San Nicolas et al., 2014). Similar features are identified in samples with 10 wt.% MK (**Figure 4B**), although the surface of this cement seems rougher than that of the slag-only binders.

Carbonation induces notable changes in the microstructures of the binders assessed. In pastes solely based on slag

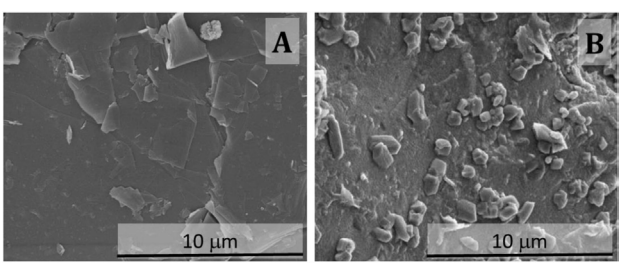

FIGURE 4 | Secondary electron micrographs of fractured sections of non-carbonated alkali-activated slag/metakaolin binders with GBFS/(GBFS + MK) ratios of (A) 1.0 and (B) 0.9.

(**Figures 5A1,A2**), the continuity of the matrix is lost upon accelerated carbonation, so that highly fragmented laminar type structures are identified throughout the sample. A clear separation between each laminar type structure is observed, which might induce an increase of the microporosity in carbonated pastes, favoring the ingress of aggressive agents through the fragmented matrix. In pastes with 10 wt.% MK (**Figures 5B1,B2**) the formation of laminar type structures throughout the matrix, along with formation of large and continuous particles, is observed. The laminar structures seem more continuous than those observed in cements without MK.

The most notable changes are identified in the carbonated pastes with 20 wt.% (**Figures 5C1,C2**). This binder shows a continuous and highly porous microstructure, with a mesh type structure, where formation of distinctive crystalline phases was not identified.

IMPLICATIONS FOR DURABILITY OF ALKALI-ACTIVATED SLAG/METAKAOLIN PASTES

One of the main threats posed by carbonation of alkali-activated reinforced concretes is a potential reduction of the alkalinity in the system, so that the pH drops to values that may induce depassivation of the steel rebars, leaving the materials vulnerable to development of corrosion processes. The carbonation of alkali-activated materials can be described as a two-step mechanism initiating with the carbonation of alkalis present in the pore solution, followed by the carbonation of the hydrated reaction products in the cementitious binder (Bernal, 2014). The type and amount of carbonation products derived from the carbonation of the pore solution in particular will significantly impact the potential extent of damage to these materials.

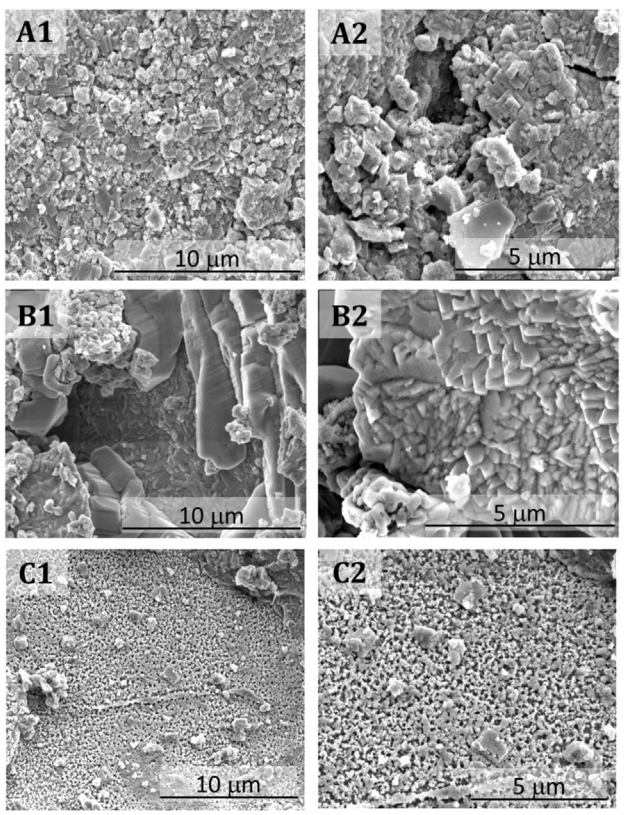

FIGURE 5 | Secondary electron micrographs of fractured carbonated alkali-activated slag/metakaolin binders with GBFS/(GBFS + MK) ratios of (A1,A2) 1.0, (B1,B2) 0.9, and (C1,C2) 0.8.

The inclusion of 10 wt.% MK in these cements does not seem to have a marked impact on the sodium carbonates derived from the carbonation of the pore solution. Conversely, in samples with 20 wt.% MK, formation of sodium carbonates is not identified, indicating that most of the alkalis have been consumed upon reaction with MK, modifying the chemistry of the pore solution. It could be then expected that the carbonation of the hydrated reaction products forming in 20 wt.% MK-containing cements will occur faster than that of cements with lower MK contents, inducing more notable microstructural changes for similar times of exposure to high CO_2 concentrations.

The continuously porous microstructure identified in the carbonated 20 wt.% MK-containing cements will aid the ingress of aggressive agents within the material, facilitating any degradation process that might take place. However, considering the reduced size of the pores identified in this cement, it might be possible that the formation and precipitation of a large amount of carbonation products could plug some of the voids, reducing the permeability of the carbonated samples, as was identified in carbonated mortar specimens produced with the same formulations as the cements assessed (Bernal, 2015). Further investigation of the physicochemical and microstructural impact of carbonation on alkali-activated slag-MK binders is required, but this paper has highlighted the importance of free alkali content in determining the mechanism and products of their carbonation.

CONCLUSION

The addition of minor fractions of MK to alkali-activated slag cements induces notable changes in the microstructure of these binders when exposed to high CO_2 concentrations. Independent of the MK content in the binders, CO_2 exposure induced decalcification of the C-(N-)A-S-H type phases present in these cements, leading to the formation of N-A-S-H type gels as the main reaction products. Similar sodium carbonates, derived from the carbonation reaction between the free alkalis in the pore solution and CO_2, are identified in pastes with up to 10 wt.% MK. The fact that alkali-rich carbonate salts, such as trona or gaylussite are not identified when higher contents of MK are added to these cements indicates that there is a reduced content of free alkalis in the pore solution, most likely as a consequence of alkali binding through reaction with MK. The reduced concentration of free alkalis in the pore solution in MK-blended alkali-activated

slag cements makes these cements more vulnerable to carbonation, as the dissolved CO_2 in pore solution will react with the hydrated binding phases, inducing a notable increase in their microporosity.

AUTHOR CONTRIBUTIONS

SB is the sole author of this paper. She produced all the samples, analyzed them using the analytical techniques described in this manuscript, processed the information, and wrote the paper.

ACKNOWLEDGMENTS

This work was supported in part by the UK Engineering and Physical Sciences Research Council through grant EP/M003272/1. Use of the Advanced Photon Source at Argonne National Laboratory (ANL) was supported by the US Department of Energy, Office of Science, Office of Basic Energy Sciences, under Contract No. DE-AC02-06CH11357. Prof. Ruby Mejía de Gutierrez (U. del Valle, Colombia), Prof. John Provis (U. Sheffield, UK), and Dr. Volker Rose (ANL, USA) are greatly acknowledged for the valuable discussions and support during the execution of this study.

REFERENCES

Alarcon-Ruíz, L., Platret, G., Massieu, E., and Ehrlacher, A. (2005). The use of thermal analysis in assessing the effect of temperature on a cement paste. *Cem. Concr. Res.* 35, 609. doi:10.1016/j.cemconres.2004.06.015

Barall, E. M., and Rogers, L. B. (1966). Differential thermal analysis of the decomposition of sodium bicarbonate and its simple double salts. *J. Inorg. Nucl. Chem.* 28, 41. doi:10.1016/0022-1902(66)80226-9

Bernal, S. A. (2014). The resistance of alkali-activated cement-based binders to carbonation in *Handbook of Alkali-Activated Cements, Mortars and Concretes*, eds F. Pacheco-Torgal, J. Labrincha, C. Leonelli, A. Palomo, and P. Chindaprasit (Cambridge: Woodhead Publishing).

Bernal, S. A. (2015). Effect of the activator dose on the compressive strength and accelerated carbonation resistance of alkali silicate-activated slag/metakaolin blended materials. *Constr. Build. Mater.* 98, 217. doi:10.1016/j.conbuildmat.2015.08.013

Bernal, S. A., Mejía de Gutiérrez, R., and Provis, J. L. (2012a). Engineering and durability properties of concretes based on alkali-activated granulated blast furnace slag/metakaolin blends. *Constr. Build. Mater.* 33, 99. doi:10.1016/j.conbuildmat.2012.01.017

Bernal, S. A., Provis, J. L., Brice, D. G., Kilcullen, A., Duxson, P., and van Deventer, J. S. J. (2012b). Accelerated carbonation testing of alkali-activated binders significantly underestimate the real service life: the role of the pore solution. *Cem. Concr. Res.* 42, 1317. doi:10.1016/j.cemconres.2012.07.002

Bernal, S. A., Mejía de Gutierrez, R., Rose, V., and Provis, J. L. (2010). Effect of silicate modulus and metakaolin incorporation on the carbonation of alkali silicate-activated slags. *Cem. Concr. Res.* 40, 898. doi:10.1016/j.cemconres.2010.02.003

Bernal, S. A., Provis, J. L., Walkley, B., San Nicolas, R., Gehman, J. D., Brice, D. G., et al. (2013a). Gel nanostructure in alkali-activated binders based on slag and fly ash, and effects of accelerated carbonation. *Cem. Concr. Res.* 53, 127. doi:10.1016/j.cemconres.2013.06.007

Bernal, S. A., Provis, J. L., Rose, V., and Mejía de Gutiérrez, R. (2013b). High-resolution X-ray diffraction and fluorescence microscopy characterization of alkali-activated slag-metakaolin binders. *J. Am. Ceram. Soc.* 96, 1951. doi:10.1111/jace.12247

Bernal, S. A., Rodríguez, E. D., Mejía de Gutierrez, R., Gordillo, M., and Provis, J. L. (2011a). Mechanical and thermal characterisation of geopolymers based on silicate-activated metakaolin/slag blends. *J. Sci. Mater.* 46, 5477. doi:10.1007/s10853-011-5490-z

Bernal, S. A., Provis, J. L., Mejía de Gutierrez, R., and Rose, V. (2011b). Evolution of binder structure in sodium silicate-activated slag-metakaolin blends. *Cem. Concr. Compos.* 33, 46. doi:10.1016/j.cemconcomp.2010.09.004

Bernal, S. A., San Nicolas, R., Myers, R. J., Mejía de Gutiérrez, R., Puertas, F., van Deventer, J., et al. (2014a). MgO content of slag controls phase evolution and structural changes induced by accelerated carbonation in alkali-activated binders. *Cem. Concr. Res.* 57, 33. doi:10.1016/j.cemconres.2013.12.003

Bernal, S. A., San Nicolas, R., Provis, J. L., Mejía de Gutiérrez, R., and van Deventer, J. S. J. (2014b). Natural carbonation of aged alkali-activated slag concretes. *Mater. Struct.* 47, 693–707. doi:10.1617/s11527-013-0089-2

Buchwald, A., Hilbig, H., and Kaps, C. (2007). Alkali-activated metakaolin-slag blends – performance and structure in dependence on their composition. *J. Sci. Mater.* 42, 3024. doi:10.1007/s10853-006-0525-6

Buchwald, A., Vanooteghem, M., Gruyaert, E., Hilbig, H., and De Belie, N. (2015). Purdocement: application of alkali-activated slag cement in Belgium in the 1950s. *Mater. Struct.* 48, 501. doi:10.1617/s11527-013-0200-8

Deja, J. (2002). Carbonation aspects of alkali activated slag mortars and concretes. *Silic. Ind.* 3–4, 37.

Farmer, V. C. (1974). *The Infrared Spectra of Minerals*. London: Mineralogical Society.

Fernández-Bertos, M., Simons, S. J. R., Hills, C. D., and Carey, P. J. (2004). A review of accelerated carbonation technology in the treatment of cement-based materials and sequestration of CO_2. *J. Hazard. Mater.* 112, 193. doi:10.1016/j.jhazmat.2004.04.019

Gadsden, J. A. (1975). *Infrared Spectra of Minerals and Related Inorganic Compounds*. London: Butterworths.

García Lodeiro, I., Macphee, D. E., Palomo, A., and Fernández-Jiménez, A. (2009). Effect of alkalis on fresh C–S–H gels. FTIR analysis. *Cem. Concr. Res.* 39, 147. doi:10.1016/j.cemconres.2009.01.003

García-Lodeiro, I., Fernández-Jiménez, A., Blanco, M. T., and Palomo, A. (2008). FTIR study of the sol–gel synthesis of cementitious gels: C–S–H and N–A–S–H. *J. Sol-Gel Sci. Technol.* 45, 63. doi:10.1007/s10971-007-1643-6

Habert, G., d'Espinose de Lacaillerie, J. B., and Roussel, N. (2011). An environmental evaluation of geopolymer based concrete production: reviewing current research trends. *J. Cleaner Prod.* 19, 1229. doi:10.1016/j.jclepro.2011.03.012

Hobbs, D. W. (2001). Concrete deterioration: causes, diagnosis, and minimising risk. *Int. Mater. Rev.* 46, 117. doi:10.1179/095066001101528420

Huang, C. K., and Kerr, P. F. (1960). Infrared study of the carbonate minerals. *Am. Mineral.* 45, 311.

Johnson, D. R., and Robb, W. A. (1973). Gaylussite: thermal properties by simultaneous thermal analysis. *Am. Mineral.* 58, 778.

Juenger, M. C. G., Winnefeld, F., Provis, J. L., and Ideker, J. (2011). Advances in alternative cementitious binders. *Cem. Concr. Res.* 41, 1232. doi:10.1016/j.cemconres.2010.11.012

L'Hôpital, E., Lothenbach, B., Scrivener, K., and Kulik, D. A. (2016). Alkali uptake in calcium alumina silicate hydrate (C-A-S-H). *Cem. Concr. Res.* 85, 122. doi:10.1016/j.cemconres.2016.03.009

Mozgawa, W., Fojud, Z., Handke, A., and Jurga, S. (2002). MAS NMR and FTIR spectra of framework aluminosilicates. *J. Mol. Struct.* 614, 281. doi:10.1016/S0022-2860(02)00262-4

Myers, R. J., Bernal, S. A., Provis, J. L., Gehman, J. D., and van Deventer, J. S. J. (2015). The role of Al in cross-linking of alkali-activated slag cements. *J. Am. Ceram. Soc.* 98, 996. doi:10.1111/jace.13360

Myers, R. J., Bernal, S. A., San Nicolas, R., and Provis, J. L. (2013). Generalized structural description of calcium-sodium aluminosilicate hydrate gels: the crosslinked substituted tobermorite model. *Langmuir* 29, 5294. doi:10.1021/la4000473

Palacios, M., and Puertas, F. (2006). Effect of carbonation on alkali-activated slag paste. *J. Am. Ceram. Soc.* 89, 3211. doi:10.1111/j.1551-2916.2006.01214.x

Provis, J. L., and Bernal, S. A. (2014). Geopolymers and related alkali-activated materials. *Annu. Rev. Mater. Res.* 44, 299. doi:10.1146/annurev-matsci-070813-113515

Puertas, F., Palacios, M., and Vázquez, T. (2006). Carbonation process of alkali-activated slag mortars. *J. Sci. Mater.* 41, 3071. doi:10.1007/s10853-005-1821-2

San Nicolas, R., Bernal, S. A., Mejía de Gutiérrez, R., van Deventer, J. S. J., and Provis, J. L. (2014). Distinctive microstructural features of aged sodium

silicate-activated slag concretes. *Cem. Concr. Res.* 65, 41. doi:10.1016/j.cemconres.2014.07.008

Sanjuán, M. A., Andrade, C., and Cheyrezy, M. (2003). Concrete carbonation test in natural and accelerated conditions. *Adv. Cem. Res.* 15, 171. doi:10.1680/adcr.2003.15.4.171

Sitarz, M., Handke, M., and Mozgawa, W. (2000a). Identification of silicooxygen rings in SiO_2 based on IR spectra. *Spectrochimica Acta A* 56, 1819. doi:10.1016/S1386-1425(00)00241-9

Sitarz, M., Handke, M., Mozgawa, W., Galuskin, E., and Galuskina, I. (2000b). The non-ring cations influence on silicooxygen ring vibrations. *J. Mol. Struct.* 555, 357. doi:10.1016/S0022-2860(00)00621-9

Williams, R. P., Hart, R. D., and van Riessen, A. (2011). Quantification of the extent of reaction of metakaolin-based geopolymers using X-ray diffraction, scanning electron microscopy, and energy-dispersive spectroscopy. *J. Am. Ceram. Soc.* 94, 2663. doi:10.1111/j.1551-2916.2011.04410.x

Yang, K., Yang, C., Magee, B., Nanukuttan, S., and Ye, J. (2016). Establishment of a preconditioning regime for air permeability and sorptivity of alkali-activated slag concrete. *Cem. Concr. Compos.* 73, 19. doi:10.1016/j.cemconcomp.2016.06.019

Yu, P., Kirkpatrick, R. J., Poe, B., McMillan, P. F., and Cong, X. (1999). Structure of calcium silicate hydrate (C-S-H): Near-, mid-, and far-infrared spectroscopy. *J. Am. Ceram. Soc.* 82, 742. doi:10.1111/j.1151-2916.1999.tb01826.x

Conflict of Interest Statement: The author declares that the research was conducted in the absence of any commercial or financial relationships that could be construed as a potential conflict of interest.